Petroleum Science 22 (2025) 1485–1496

Contents lists available at ScienceDirect

Petroleum Science

journal homepage: www.keaipublishing.com/en/journals/petroleum-science

Original Paper

Intermediate-high frequency dielectric permittivity of oil-wet rock and the wettability characterization

Pei-Qiang Zhao [a, b, *], Yu Chen [c], Yu-Ting Hou [d], Xiu-Ling Chen [e], Wei Duan [a, b], Shi-Zhen Ke [a, b]

[a] State Key Laboratory of Petroleum Resources and Engineering, China University of Petroleum (Beijing), Beijing, 102249, China
[b] Beijing Key Laboratory of Earth Prospecting and Information Technology, China University of Petroleum (Beijing), Beijing, 102249, China
[c] Geological Exploration and Development Research Institute, CNPC Chuanqing Drilling Engineering Co., Ltd., Chengdu, 610056, Sichuan, China
[d] PetroChina Changqing Oilfield Company, Xi'an, 710018, Shaanxi, China
[e] Third Gas Extraction Plant, PetroChina Changqing Oilfield Company, Ordos, 017300, Inner Mongolia, China

ARTICLE INFO

Article history:
Received 19 June 2024
Received in revised form
28 October 2024
Accepted 6 February 2025
Available online 8 February 2025

Edited by Meng-Jiao Zhou and Teng Zhu

Keywords:
Wettability
Dielectric permittivity
NMR T_2 spectra
Simulated annealing

ABSTRACT

Wettability has complex effects on the physical properties of reservoir rocks. The wettability of rocks should be characterized accurately to explore and develop oil and gas. Researchers have studied the rock wettability by dielectric spectra which contained abundant information. To study the rock wettability from dielectric dispersion, four rock samples with different wettabilities were used to design an experimental measurement flow. The relative dielectric permittivity in the frequency range of 100 Hz–10 MHz and nuclear magnetic resonance T_2 spectra of the samples were obtained. Subsequently, the wettabilities of the rocks were verified by the T_2 spectra. The dielectric dispersions of the samples under different conditions were analyzed. Furthermore, the simulated-annealing (SA) algorithm was used to invert the wettability and related parameters of the rocks by a dielectric dispersion model. The results indicated that the dielectric permittivity of lipophilic rocks is lower than that of hydrophilic rocks, and that the dielectric permittivity of hydrophilic rocks decreases faster as the frequency increases. The dielectric permittivity in the high-frequency band is associated with the water content. The rock wettability parameters obtained via inversion agreed well with the T_2 spectra, and the saturation index of the rocks. The errors between the rock permittivity calculated by the inverted parameters and the experimentally measured values were minor, indicating that rock wettability could be accurately characterized using dielectric dispersion data.

1. Introduction

With the exploration and development of unconventional reservoirs, numerous oil-wet and mixed-wet reservoirs have been discovered, such as unconventional tight sandstone reservoirs in the Triassic Yanchang Formation of the Ordos Basin (Feng et al., 2017) and shale reservoirs in the Paleogene Shahejie Formation of the Bohai Bay Basin (Hu et al., 2018). Wettability is a crucial parameter for investigating the formation mechanism of oil and gas reservoirs and increasing their development efficiency. Accurate characterization of wettability is an important step in the exploration and development of unconventional reservoirs. There are several methods for characterizing rock wettability in the laboratory. Typically, the Amott index method and the contact-angle method characterize the wettability of rocks. The resistivity measurements could also indicate wettability (Mungan and Moore, 1968; Newgord et al., 2018, 2019). Nuclear magnetic resonance (NMR) measurement is another alternative method for characterizing the wettability of rocks (Looyestijn and Hofman, 2005, 2008; Liang et al., 2023a, 2023b; Jia et al., 2024). Characterizations of wettability by resistivity and NMR measurements are semi quantitative, and the measurement process are extremely complicated. Also, researchers have attempted to characterize rocks' wettability using the dielectric spectra (Toumelin et al., 2005; Seleznev and Habashy, 2016). Wettability controls the distribution and connectivity of fluid in pores, and the pore throats between oil-wet particles are easily filled with oil, which will change the electrical response of the porous system, thereby affecting the polarizability

* Corresponding author.
E-mail address: pqzhao@cup.edu.cn (P.-Q. Zhao).

https://doi.org/10.1016/j.petsci.2025.02.001

of the rock particle surface (Capaccioli et al., 2000). Thus, wettability is an essential factor that controls the dielectric dispersion of rocks (Nguyen et al., 1999; Bona et al., 2002; Al-Ofi et al., 2017).

The preliminary research mainly focuses on qualitative analysis of the influence of wettability on dielectric constant. Knight and Abad (1995) measured the dielectric constants of hydrophobic sandstone at a frequency of 1 MHz and found that the wettability affected the dielectric constant. Bona et al. (1998) measured the relative permittivity of the glass filters and Berea sandstone samples in the range of 100 Hz–40 MHz. The results indicated that both the real and imaginary parts of the permittivity of a water-wet sample were higher than those of an oil-wet sample. Additionally, the dispersivity and loss tangent were proven to be the most suitable parameters for distinguishing the wettability of the samples. Bona et al. (1999, 2002) and Capaccioli et al. (2000) measured the dielectric permittivity of glasses filters, Berea sandstone and reservoir samples and increased the maximum measurement frequency to 10 GHz. The results indicated that at the same level of saturation, the relative permittivity of water-wet samples decreased more significantly than those of oil-wet rocks as frequency increases. Also, the dielectric dispersion of rocks was affected by the wettability over the entire frequency range and that the dielectric dispersion mechanism in the gigahertz frequency range was little affected by water saturation were concluded. Nguyen et al. (1999) measured the complex permittivity of water-wet and oil-wet unconsolidated quartz samples in the frequency range of 0.3 MHz–1.5 GHz. The results indicated that the relative permittivity of the oil-wet sample was lower than that of water-wet rocks when the water saturation was very low or high. Gkortsas et al. (2015) studied the wettability from dielectric measurements on rocks using the Feng-Sen model (Feng and Sen, 1985). They found the shape factor defined in the Feng-Sen model has a higher value for mixed-wet rocks than water wet rocks. The above studies did not characterize wettability quantitatively.

Recently, Garcia and Heidari (2018) and Jin et al. (2020a) proposed quantitative evaluation methods for wettability. Garcia and Heidari (2018) characterized the surface permittivity of grains in the wetting phase using the solid-liquid electric double layer theory and calculated the relative permittivity of whole grains by introducing a fractional wettability index (X_w). The relative permittivity of the fluids was calculated using the capacitance-layer thickness, saturation, and porosity of the oil-water interface. Finally, according to the grains and fluid phase, the relative permittivity of fluid-filled rocks was calculated using the effective medium model or the Hanai-Bruggeman formula. Subsequently, Garcia et al. (2019) used a combination of downhill gradient-descent and evolutionary methods to invert rock wettability and water saturation. Considering the interfacial polarizability between a pore surface and fluid, Jin et al. (2020a) established a mechanistic model to quantify the effects of the wettability (i.e., contact angle) of conductive particles (i.e., pyrite particles in the shale). In this model, the wettability of conductive mineral particles of rocks are characterized by a contact angle. The dispersion of the electrical conductivity and permittivity in the frequency range of 100 Hz–10 MHz of the porous media were simulated numerically. The effect of mixed wet clay minerals was considered on the basis of an existing model (Jin et al., 2020b). The simulation was similar to previous measurements in the range of 100 Hz–10 MHz. At approximately 1 GHz, the effect of the wettability on the permittivity was negligible. However, this model considers the impact of wettability when the rock contains conductive minerals.

In this study, we drilled rock samples from the Jurassic Yan'an Formation in Ordos Basin, China. Rock samples with different wettabilities and saturation levels were prepared via an experimental design. The NMR T_2 spectra, and dielectric constant in the range of 100 Hz–10 MHz of rocks under different conditions were measured. The NMR T_2 spectra were used to assess the rock wettability qualitatively. And the effects of wettability and water saturation on rock dielectric dispersion were analyzed. Based on the dielectric dispersion model of Garcia and Heidari (2018), a global optimization algorithm (simulated-annealing, SA) was used to invert the wettability and related rock parameters. The rock wettability parameters obtained via inversion agreed well with the T_2 spectra, indicating that rock wettability can be accurately characterized using dielectric dispersion data. Compared with traditional methods, the quantitative characterization method established could quickly analyze the wettability of particles on the surface inside the rock, and the measurement is easy to perform.

2. Samples and experiments

In this study, four samples were drilled from the Jurassic Yan'an Formation in the Pengyang area of the Ordos Basin. The Pengyang area is located in the southern Tianhuan Depression of the basin. The studied formations focused on the Yan6, Yan8 and Yan9 oil members of the Yan'an Formation. The lithologies of the reservoirs are dominated by lithic feldspar sandstone with high maturity of composition, general sorting and grinding, and strong diagenesis. The oil accumulation of the Yan'an Formation was very complicated (Tong, 2016). It went through the process of accumulation, destruction, and re-accumulation, resulting in a set of complicated wettability of reservoirs. This area has abundant well log data, including conventional logs, NMR and dielectric logs. The reservoirs with "abnormal" overlapping of compensated neutron and bulk density (CNL and DEN) logs are oil-wet, and those with "normal" overlapping of CNL and DEN logs have water-wet wettability (Wang, 2022; Zhao et al., 2023).

The four sandstone samples were from four different wells. The samples were labeled ZY4-34, ZY3-14, ZY2-16, and ZY5-3. Each sample had a diameter of 25.4 mm. The original wettability of ZY5-3 is water-wet, and the other three samples are oil-wet. ZY3-14 and ZY2-16 were cut into two parallel samples, i.e., A and B, respectively. Samples A were not subjected to cleaning to maintain its wettability, whereas samples B was subjected to cleaning prior to resistivity measurement for comparative analysis. ZY4-34 was not cut into parallel samples, the symbols α and β were used to distinguish the different treatments. ZY5-3 was used as a comparison sample, and its properties were measured after cleaning. Table 1 presents the pre-treatment for the rock samples. The pictures of ZY5-3, ZY3-14A and ZY3-14B, ZY4-34 are shown in Fig. 1.

Since the majority of the formation water type in the research area is calcium chloride solution, to make the research more in line with the actual geological conditions, we chose to use the $CaCl_2$ solution. Samples ZY2, ZY5, ZY4, and ZY3 were filled with $CaCl_2$ solution at concentrations of 3000, 6000, 20000, and 90000 ppm, respectively. The crude oil used in the sample was extracted from the target layer. The NMR bulk relaxation of the oil was measured.

Table 1
Pretreatment of the rock samples.

Sample	Length, cm	Cut	Cleaning	Wettability
ZY3-14A	4.57	Cut into two samples	No	Oil-wet
ZY3-14B	3.98		Yes	Verification required
ZY4-34α	3.94	No	No	Oil-wet
ZY4-34β	3.94		Yes	Verification required
ZY2-16A	3.12	Cut into two samples	No	Oil-wet
ZY2-16B	3.17		Yes	Verification required
ZY5-3	3.74	No	Yes	Water-wet

Fig. 1. Pictures of core samples. From top to bottom: ZY5-3, ZY3-14A and ZY3-14B, ZY4-34.

The experimental process is illustrated in Fig. 2. Six electric resistivity spectra and twelve NMR T_2 spectra of samples were obtained.

The porosity and permeability were measured via the helium method using a helium porosimeter under the China Industrial Standard GB/T 29172-2012 for core analysis. Geospec2 (Oxford Instruments) with a magnetic-field intensity of 2 MHz was used to perform NMR measurements. During the measurements, the waiting time (T_W) was set as 3s, the echo interval was 0.2 ms, the number of echoes was 4000, and the number of scans was 64. The method proposed by Butler et al. (1981) was used for inversion of the T_2 spectra. The T_2 range and number of data points were set as 0.01–10000 ms and 128, respectively. The cation exchange capacity (*CEC*) was measured following the China Standard SY/T 6352-2013. The relative permittivity of the rock was determined by measuring the complex conductivity of the rock using an HP4294 impedance analyzer. A schematic of the measurement is shown in Fig. 3. This measurement is carried out under normal temperature and pressure conditions, usually selecting a pressure of 1 MPa–3 MPa (Li et al., 2019; Wei et al., 2024). The temperature and pressure were 25 °C and 1.01 MPa, respectively. The bipolar measurement method was used, and the frequency range was 100 Hz–100 MHz. The rock permittivity was calculated as follows (Börner et al., 2015; Niu et al., 2020):

$$\sigma_j^* = \sigma_j + i\sigma_j'' \tag{1}$$

$$\varepsilon_r = \frac{\sigma_j''}{\omega\varepsilon_0} \tag{2}$$

where σ_j^* represents the complex conductivity of the rock, S/m; σ_j is

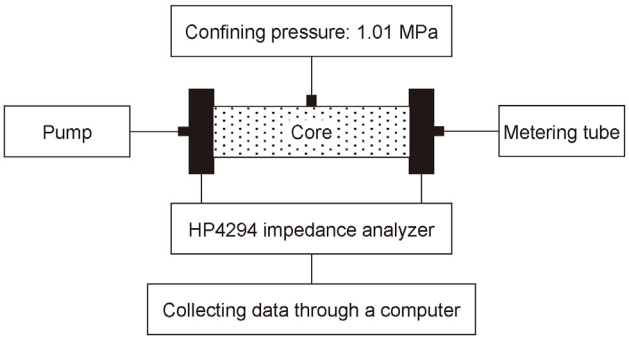

Fig. 3. Schematic of the measurement system (modified after Li et al., 2019).

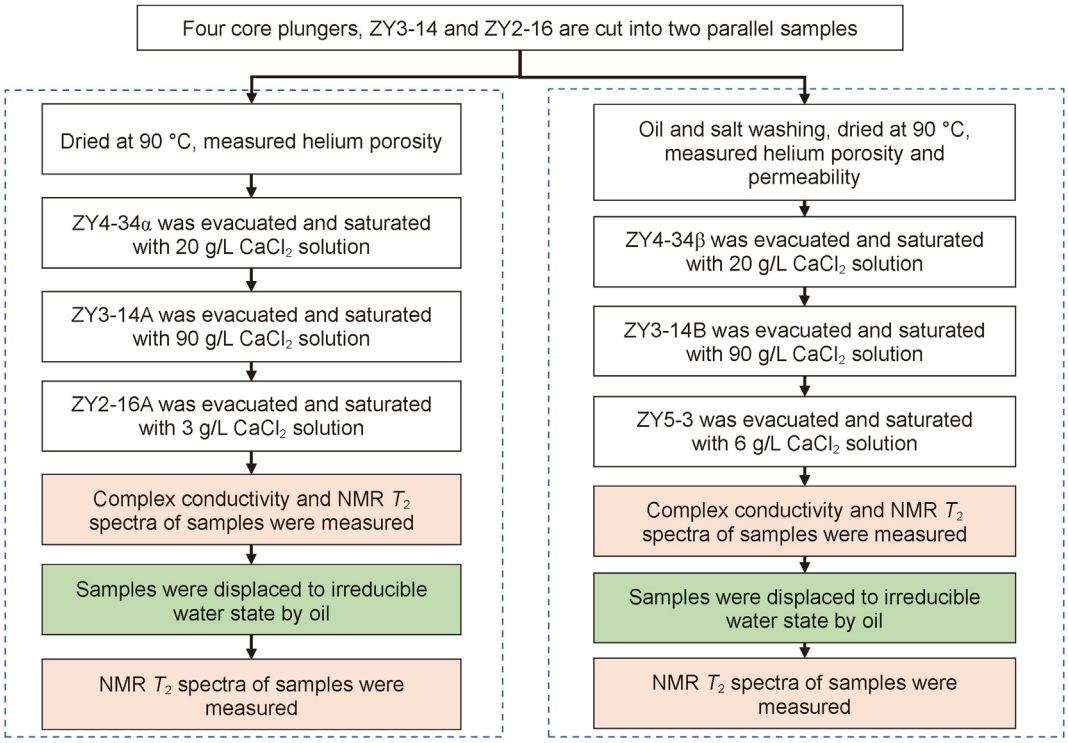

Fig. 2. Experimental flowchart.

the real part of the rock conductivity, S/m; σ_j'' is the imaginary part of the rock conductivity, S/m; ε_r is the relative permittivity of the rock; ε_0 represents the permittivity of free space (8.854×10^{-12} F/m); ω represents the angular frequency, rad/s; and i is the imaginary unit. Besides, the permittivity was also corrected by a simple method.

As the sample without cleaning contained residual oil, the water saturation of samples A and α had to be corrected. The correction formula is shown as

$$S_{wr} = S_{wA}\frac{\phi_A}{\phi_B} \tag{3}$$

where S_{wr} represents the actual water saturation of sample A, v/v; S_{wA} represents the water saturation of the samples before cleaning, v/v; ϕ_A represents the porosity of the samples before cleaning, v/v; and ϕ_B represents the porosity of the samples after cleaning, v/v.

3. Data processing method

3.1. Model

Garcia and Heidari (2018) proposed a dielectric dispersion model containing the wettability. The model consisted of three parts. The electric double layer theory of the solid-liquid interface was used to characterize the dielectric dispersion characteristics of water-wet rock grains. The capacitance-layer theory for oil-water two-phase fluids was used to characterize the dielectric dispersion characteristics of the liquid phases. Effective medium models (the Maxwell Garnett or Hanai-Bruggeman model) were used to calculate the dielectric dispersion of fluid-filled rocks.

3.1.1. Characterization of dielectric permittivity of grains

Mixed-wet rocks contain water-wet and oil-wet grains. A fractional wettability index X_w was introduced to indicate the proportions of the oil-wet and water-wet components. When the rock is entirely lipophilic, $X_w = 0$, and when the rock is entirely hydrophilic, $X_w = 1$. The relative permittivity of the grains can be expressed using the Maxwell Garnett or Hanai-Bruggeman model, as shown as follows (Garcia and Heidari, 2018):

$$\varepsilon_{solid} = \varepsilon_{SC} + (1 - X_w)\varepsilon_{SC}\frac{\varepsilon_g - \varepsilon_{SC}}{\varepsilon_{SC} + X_w N_g(\varepsilon_g - \varepsilon_{SC})} \tag{4}$$

$$\frac{\varepsilon_g - \varepsilon_{solid}}{\varepsilon_g - \varepsilon_{SC}} = X_w\left[\frac{\varepsilon_{solid}}{\varepsilon_{SC}}\right]^{N_g} \tag{5}$$

where N_g is the depolarization factor of the water-wet grains, which is related to the particle shape; ε_g represents the relative permittivity of the mineral constituent of the grains, F/m; ε_{SC} represents the relative permittivity of the grains with an electric double layer, which is calculated as

$$\varepsilon_{SC} = \frac{\sigma_S}{j\omega\varepsilon_0} + \varepsilon_g \tag{6}$$

where σ_S represents the complex surface conductivity of spherical grains in an electrolyte, which can be calculated as

$$\sigma_S = \frac{2}{r}\left(\sum_{ST} + \sum_{S0}\right) - \frac{2}{r}\frac{\sum_{ST}}{1 + (j\omega\tau_0)^c} \tag{7}$$

where r represents the radius of the grain, μm; $\sum_{ST}$ and $\sum_{S0}$ represents the contribution of the Stern layer and the frequency-independent contribution to the complex surface conductance, respectively, S/m^2; τ_0 represents the relaxation time; and c is the Cole–Cole exponent. The parameters are calculated as follows:

$$\sum_{ST} = z\beta_{ST}\alpha_{ST}\rho_g f_m CEC \tag{8}$$

$$\sum_{S0} = z\beta_0\alpha_0\rho_g(1 - f_m)CEC \tag{9}$$

$$\tau_0 = \frac{ezr^2}{2Mk_BT\beta_{ST}} \tag{10}$$

where z represents the valence of the counterions; β_{ST} and β_0 represent the ion mobilities in the Stern and Gouy-Chapman layers, respectively, m^2/sV; α_{ST} and α_0 are coefficients related to the geometry of the Stern and diffuse layers, respectively; ρ_g represents the grain density, g/cm^3; f_m is the fraction volume of counterions present in the Stern layer; CEC represents the cation exchange capacity, C/kg; e represents the elementary charge (1.60×10^{-19} C); M is a correction term for the diffuse layer to the dielectric dispersion; and k_B is the Boltzmann constant (1.38×10^{-23} m^{2}kg/s^{2}K).

3.1.2. Characterization of relative permittivity of fluids

The characterization of relative permittivity of the fluids was similar to those of the grains. The Maxwell Garnett model (or Hanai-Bruggeman model) was used to calculate the effective permittivity of the fluids (Garcia and Heidari, 2018):

$$\varepsilon_{fluid} = \varepsilon_w + (1 - S_w)\varepsilon_w\frac{\varepsilon_{HC,C} - \varepsilon_w}{\varepsilon_w + S_w N_{HC,C}(\varepsilon_{HC,C} - \varepsilon_w)} \tag{11}$$

where S_w represents the water saturation, v/v; ε_w represents the relative permittivity of water, which is calculated using the method proposed by Stogryn (1971); $N_{HC,C}$ is the depolarization factor associated with the hydrocarbon phase; and $\varepsilon_{HC,C}$ represents the effective permittivity of the hydrocarbon phase, which can be calculated as

$$\varepsilon_{HC,C} = \varepsilon_C\frac{2(1 - v)\varepsilon_C + (1 + 2v)\varepsilon_{HC}}{(2 + v)\varepsilon_C + (1 - v)\varepsilon_{HC}} \tag{12}$$

Here, ε_C represents the permittivity of the inner layer at the hydrocarbon-water interface, F/m; ε_{HC} represents the permittivity of the bulk hydrocarbon phase, and v represents the volume fraction of the capacitance layer relative to the hydrocarbon phase, which can be respectively calculated as

$$\varepsilon_{HC} = 2 + j\frac{\sigma_{HC}}{\omega\varepsilon_0} \tag{13}$$

$$v = \left(1 - \frac{h}{r_0}\right)^3 \tag{14}$$

where, σ_{HC} represents the conductivity of the hydrocarbon, S/m; h represents the thickness of the inner layer, nm; and r_0 represents the radius of the hydrocarbon droplet, μm.

3.1.3. Characterization of relative permittivity of fluid-filled rocks

The Maxwell Garnett model (or Hanai-Bruggeman model) was used to calculate the effective permittivity of fluid-filled rocks combining grains and fluids (Garcia and Heidari, 2018):

$$\varepsilon_R = \varepsilon_{fluid} + (1-\phi)\varepsilon_{fluid}\frac{\varepsilon_{solid} - \varepsilon_{fluid}}{\varepsilon_{fluid} + \phi N_f\left(\varepsilon_{solid} - \varepsilon_{fluid}\right)} \quad (15)$$

where ϕ represents the porosity, v/v; N_f is the depolarization factor associated with the fluid phase.

The model considers the effects of the grain phase, fluid phase, and physical structure on the relative permittivity of rocks and accurately characterizes the dielectric properties of reservoir rocks in the frequency range of 100 Hz–10 MHz.

The objective function f in this paper was defined as

$$f = 100 \times \sqrt{\|\ln(d_m) - \ln(\widehat{d})\|_2^2} \quad (16)$$

where d_m represents the measured value, $\widehat{d}$ represents the value calculated by the model; $\|\cdot\|_2^2$ represents the L_2 norm.

It reduced the impact of multiple orders of magnitude differences in permittivity in this frequency range on calculations.

3.2. SA algorithm

To avoid solutions falling within a local range, a global simulated annealing algorithm was selected in this study. The SA algorithm had various applications in the field of geophysics, such as well logging, gravity and electromagnetic data inversion. Zhou et al. (2021) proposed a method for extraction of wave slowness of array acoustic logging components based on SA algorithm. Prasad (1999) and Xu et al. (2023) applied the SA to electromagnetic data inversion. Netto and Dunbar (2019), and Jiang and Wang (2024) used this algorithm to inverse the subsurface parameters by gravity data. Chen et al. (2011) used the nonlinear SA method to achieve joint inversion of magnetotelluric and seismic data, effectively improving the stability of the solution. The SA algorithm is based on the operation rules of the hill-climbing algorithm, which is similar with the natural annealing of crystals. The process involves heating an object to a sufficiently high temperature and cooling it gradually. During the cooling process, the particles gradually transform from disordered to ordered, reaching equilibrium at each temperature until the ground state is attained at room temperature. The algorithm has a time-varying probability of accepting new solutions and approaches zero in the search process to avoid falling into a local optimal solution. Fig. 4 shows a flowchart of the SA algorithm.

The initial parameter vector X_0 must be estimated before the algorithm is executed, which significantly affects its rate of convergence. In this paper, the initial temperature parameter was set as 200 °C, and the number of iterations at each temperature was 150 °C. The Metropolis criterion was used as the probability function for accepting the new solutions. The probability is expressed as (Metropolis et al., 1953)

$$P = \exp\left(-\frac{f(x_{new}) - f(x_{old})}{k_B T}\right) \quad (17)$$

where x_{new} is the new solution generated by disturb; x_{old} is the previous solution; k_B is the Boltzmann constant and T represents the temperature (°C) of the object, which gradually decreases from the initial value when the algorithm is executed. A random value *ran* between 0 and 1 is compared with the probability P. If $P \geq ran$, the perturbed solution is accepted as a new solution; otherwise, it is rejected. According to the Metropolis criterion, when the temperature T decreases as the number of iterations increases, the probability of an unsatisfactory perturbation solution being accepted as a new solution decreases to 0.

After each sample was inverted, the relative permittivity was recalculated using the inverted parameters, and the relative error e_r was defined to test the effectiveness of the inversion.

$$e_r = \frac{\sum|\log_{10}(d_m) - \log_{10}(\widehat{d})|}{\sum \log_{10}(d_m)} \times 100\% \quad (18)$$

4. Results

4.1. Measured physical parameters of samples

The measured parameters for the sample are presented in Table 2. After cleaning, the porosity of the samples was between 14.78% and 17.57%, whereas the permeability was between 100 and 300 mD, except for sample ZY3-14B. The porosities of samples ZY2-16A and ZY2-16B differed significantly, indicating that the residual oil contents of these samples were high, whereas those of samples ZY3-14 and ZY4-34 were low. The conductivities of different solutions varied significantly and were used to determine the relative permittivity of the aqueous solution.

4.2. Wettability analysis based on NMR T_2 spectra

Studies have clarified the basic principle of NMR for indicating rock wettability (Looyestijn and Hofman, 2005; Kuang et al., 2020). The explanation will not be repeated here. Fig. 5 show the T_2 spectra of the four samples measured under different conditions. The symbols “WS” and “OD” denote the water-saturated and oil-displaced states, respectively. According to Zhao et al. (2023), samples ZY4-34, ZY3-14, and ZY2-16 were preliminarily identified as oil-wet rocks, and ZY5-3 was identified as a water-wet sample.

The peak value of T_2 in the saturated state of sample ZY4-34α was greater than 1000 ms, whereas that after oil displacement was approximately 300 ms. This indicated that the rock has oil-wet surfaces, the T_2 relaxation of the water-saturated sample was primarily contributed to the bulk relaxation of water, and the T_2 relaxation of the rock after oil displacement was primarily contributed to the surface and bulk relaxation of oil. ZY4-34β exhibited similar characteristics after cleaning, but the peak value of T_2-WS was slightly lower than that of ZY4-34α. The T_2-OD peak value of ZY4-34β was slightly higher than that of ZY4-34α, indicating that the sample remained oil-wet after the cleaning. For sample ZY3-14A before cleaning, the T_2 in the OD state was shifted forward compared with that in the WS state, indicating its oil-wet property. However, owing to the low permeability of this sample, the T_2 peak value was lower than that for ZY4-34. After cleaning, the T_2 distribution in the OD state for sample ZY4-34B was shifted backward compared with that in the WS state, indicating that the wettability of the rocks was changed after the cleaning, and that the samples changed from oil-wet to water-wet.

Sample ZY2-16A contained a significant amount of residual oil, which filled approximately 50% of the total pores. After pressurization and saturation, the peak value on the right side of the NMR T_2 spectrum was approximately 1000 ms, and the peak value on the left side corresponded to that of the residual oil signal. After oil displacement occurred, the peak on the right side disappeared, indicating that the sample was oil-wet. The peaks on the right side for ZY5-3 in the OD and WS states were close, and they were positioned close to that corresponding to the bulk relaxation of oil, indicating that the oil in the sample underwent bulk relaxation, and that the sample was water-wet.

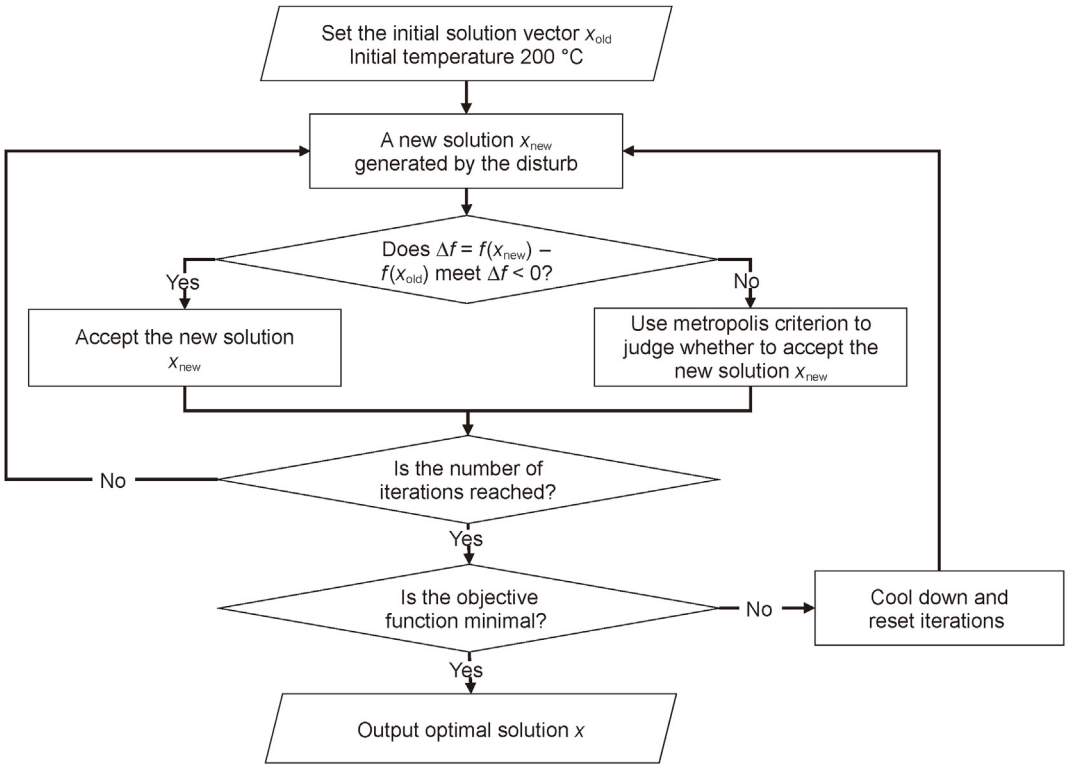

Fig. 4. Flowchart of the SA algorithm.

Table 2
Physical properties of the rock samples.

Sample	Por, %	Perm, mD	S_w, v/v	σ_w, S/m	*CEC*, C/kg	ρ_g, g/cm^3
ZY3-14A	14.35	/	0.97	9.15	1800	2.65
ZY3-14B	14.78	9.11	1.0			
ZY4-34α	15.04	/	0.88	2.97	380	2.65
ZY4-34β	17.15	272.97	1.0			
ZY2-16A	8.91	/	0.51	0.49	385	2.64
ZY2-16B	17.57	277.7	1.0			
ZY5-3	17.62	164.76	1.0	0.80	1956	2.64

4.3. Effect of wettability on permittivity

Fig. 6 shows the relative dielectric curves of samples ZY3-14 and ZY4-34 with different wettabilities in the saturated state. When the sample was saturated with water, the wettability of ZY3-14A was oil-wet, and the water saturation S_w was 0.97. As indicated by the NMR T_2 spectra above, the wettability of ZY3-14B have changed to water-wet after cleaning. At frequencies lower than 10 kHz, the relative permittivity of the water-saturated water-wet sample exceeded that of the water-saturated oil-wet sample (Fig. 6(a)). Meanwhile, the change rate of the relative permittivity of the water-wet sample at frequencies lower than 1 MHz exceeded that of the oil-wet sample. This is because the rock wettability controls the connectivity of water in pores at low frequencies, resulting in different polarizability at the interface between the rock and fluids. Due to the different conductivity between rock particles, oil phase, and water phase, charge accumulation occurs at the solid-fluid or fluid-fluid interface, resulting in polarization. The degree of charge accumulation affects the strength of the interface polarization effect. In terms of wettability, the electrical conductivity of oil is low, and the accumulated charges on the surface area of the oil phase at the solid-liquid interface of oil wet rocks are very small, resulting in weak interface polarization effects. In fact, the interface polarization effect of oil wet rocks is only partially affected by the polarization effect of hydrophilic interfaces. Therefore, the dielectric permittivity of oil wet rocks at low frequencies is lower than that of water wet rocks. Although samples ZY4-34α and ZY4-34β were both oil-wet, ZY4-34β was slightly more water-saturated (Fig. 6(b)). The S_w values of the two states were 88% and 100%, respectively. When the wettability change was insignificant, the difference between the declining slopes of the relative permittivity of the samples in the two states at frequencies lower than 10 kHz was small.

At frequencies higher than 10 kHz, the change characteristics of the permittivity differed between the two rock samples. The relative permittivity of ZY3-14A exceeded that of ZY3-14B, in contrast to the low-frequency characteristics. The relative permittivity of ZY4-34α and ZY4-34β were consistent, possibly owing to the differences in the water contents of the samples in the two states. When the rock was utterly saturated, no oil-water interface emerged, and the Maxwell-Wagner-Sillars polarizability did not occur; the relative permittivity of the sample containing oil (ranging between 10 kHz and 1 MHz) might be slightly higher than that of the water-saturated sample (Nguyen et al., 1999). This could be concluded the relative permittivity of the sample at higher frequencies are mainly attributed to porosity and water saturation, and less affected by wettability.

4.4. Verification of inversion algorithm for dielectric model

To test the inversion algorithm, we assumed a set of parameters with five different X_w values to calculate five relative permittivity curves within the band of 100 Hz–10 MHz. The X_w value was set as 0.1, 0.3, 0.5, 0.7, and 0.9, while the other parameters were fixed. The assumed parameters are presented in Table 3. We added 10% Gaussian noise to the five modeling curves, as shown in Fig. 7. For

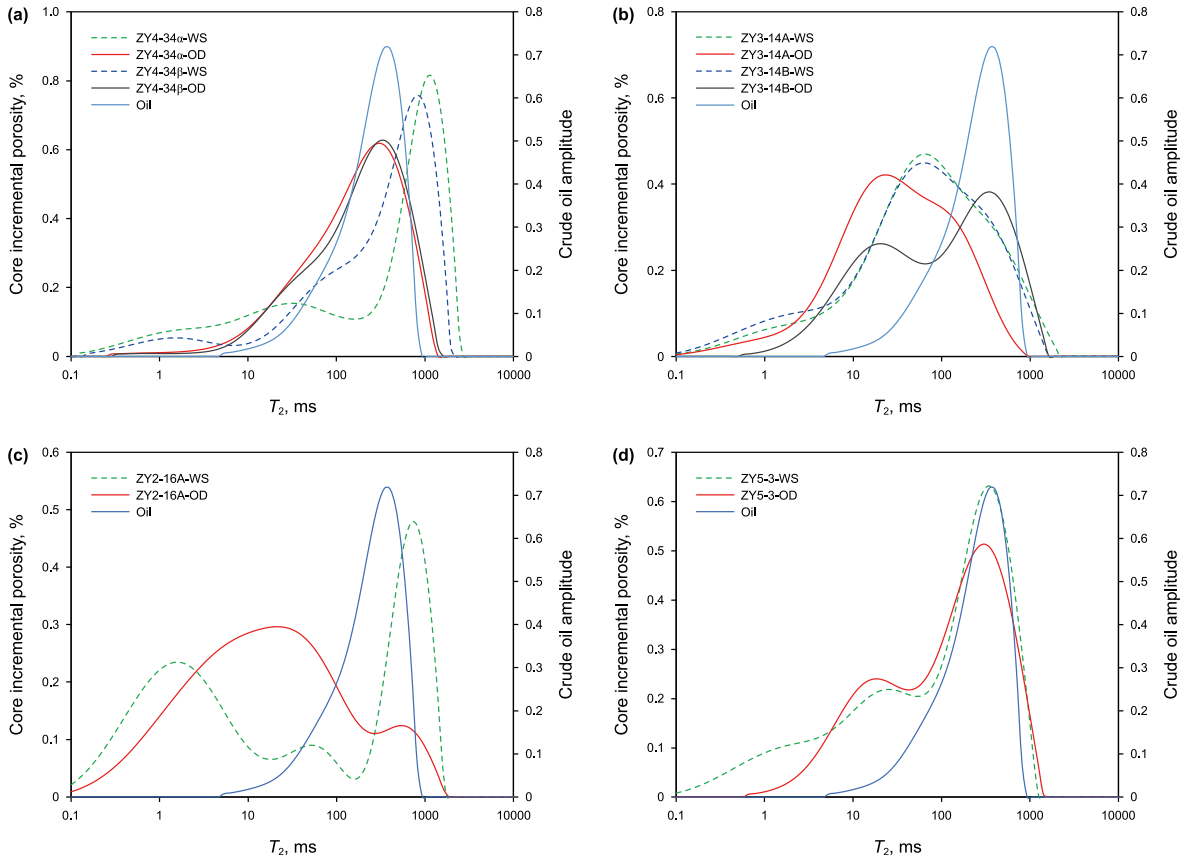

Fig. 5. T_2 spectra of the four samples measured under different conditions. **(a)** NMR T_2 spectra of ZY4-34. α and β denote non-cleaned and cleaned samples, respectively. The T_2 peaks of this sample in the OD state were shifted to left compared with those in the WS state, indicating that oil-wet surfaces existed in the pores. **(b)** NMR T_2 spectra of ZY3-14. Samples A and B were non-cleaned and cleaned, respectively. The T_2 spectra for sample A in the OD state was shifted to the left compared with that in the WS state. The T_2 spectrum for sample B in the OD state was shifted to the right compared with that in the WS state. Sample A was oil-wet, whereas sample B have changed to be water-wet. **(c)** NMR T_2 spectra of ZY2-16A. This sample was not subject to cleaning. The main T_2 peak for the sample in the OD state was shifted to the left side compared with that in the WS state, indicating that the sample was oil-wet. **(d)** NMR T_2 spectra of ZY5-3. The main T_2 peaks for the sample in the OD and WS states were close and were positioned close to the bulk relaxation of oil, indicating that the sample was water-wet.

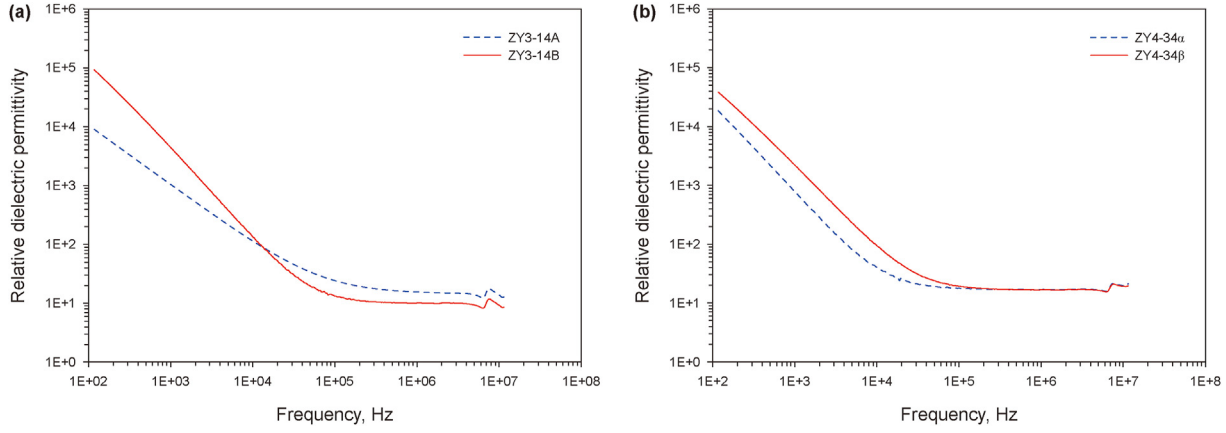

Fig. 6. Relative dielectric permittivity of water-saturated rocks with different wettabilities. Samples A and α were not cleaned. Samples B and β were cleaned. **(a)** Sample ZY3-14. **(b)** Sample ZY4-34.

the assumed cases with $X_w = 0.1$ and 0.3, the permittivity curves when the frequency was less than 10^6 Hz were significantly lower. When the wettability becomes more water-wet, i.e. $X_w > 0.5$, the sensitivity of the relative permittivity to wettability decreases with an increase in water-wet ratio. This makes the three curves for $X_w \geq 0.5$ have a small degree of separation.

We used the SA algorithm to process the synthesized curves. During the inversion process, the porosity, saturation, water conductivity, *CEC*, and grain density are known. The thickness of the inner layer h is meaningless if the hydrocarbon conductivity is 0, which is because the electric charges are not accumulated at the hydrocarbon-water interface. In addition, z represents the valence

Table 3
Assumed values for modeling the permittivity.

Parameter	Symbol	Unit	Assumed values
Ion mobility in the Stern layer	β_{ST}	m^2/sV	$5.2e^{-9}$
Ion mobility in the Gouy–Chapman layer	β_0	m^2/sV	$5.2e^{-8}$
Coefficient associated with the geometry of the Stern layer	α_{ST}	/	1.5
Coefficient associated with the geometry of the diffuse layer	α_0	/	4
Radius of the grains	r	μm	90
Depolarization factors for hydrocarbon, fluid, and grains	$N_{HC,C}, N_f, N_g$	/	1/3
Radius of the hydrocarbon droplets	r_0	μm	1
Thickness of the inner layer	h	nm	2
Fraction of counterions present in the Stern layer	f_m	/	0.95
Valence of the counterions	z	/	2
Correction term	M	/	1
Permittivity of the grains	ε_g	F/m	4.5
Density of the grains	ρ_g	g/cm^3	2.65
Cation exchange capacity	CEC	C/kg	385
Water saturation	S_w	v/v	0.35
Porosity	ϕ	v/v	0.25
Effective conductivity of the solution	σ_w	S/m	11
Effective conductivity of the hydrocarbon	σ_{HC}	S/m	0

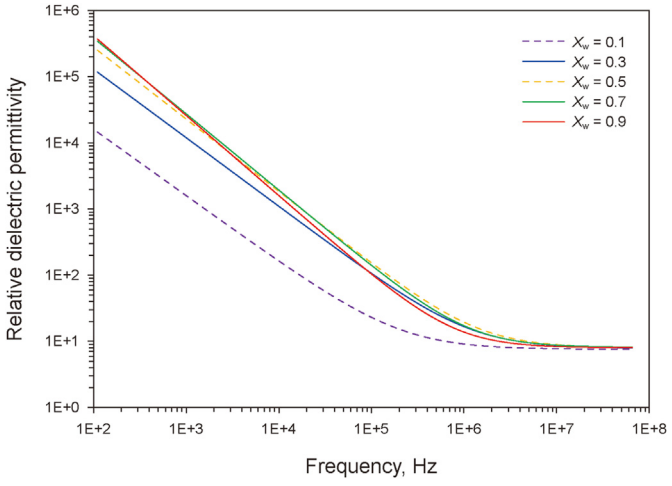

Fig. 7. Modeling curves for different X_w values. For $X_w < 0.5$, the permittivity curves when the frequency is $< 10^6$ Hz are lower.

of the counterions, which is 2 for $CaCl_2$ by definition. The range of the partition coefficient f_m is narrow, with values of 0.95 for NaCl and 0.94 for KCl (Revil and Leroy, 2004); in this study, it was 0.95. Furthermore, M is a correction term accounting for the influence of the diffuse layer, equal to 1 for low salinity and 3 for high salinity (Niu and Revil, 2016). The radio of hydrocarbon droplets is commonly in the range of 1–10 μm. For each of the five cases, we assumed r_0 to be 1 and 10 μm for calculating twice. The results indicated that the difference between the two X_w values was less than 0.01. Those parameters are not sensitive to the fractional wettability X_w. Therefore, in addition to X_w, the parameters for ion mobilities, i.e., β_0 and β_{ST} for the Gouy-Chapman and Stern layers; the geometric coefficients of the dual layers, i.e., α_{ST} and α_{S0}; and the depolarization factors for grains, hydrocarbon, and fluids should be inversed.

Table 4 presents the assumed and inverted parameter values. For each parameter, the inverted value varied, but the average of the inverted values (five times) was close to the assumed value. Fig. 8 shows a comparison of the assumed and inverted X_w values, which agreed well, confirming the effectiveness of the inversion algorithm.

4.5. Characterization of wettability

To quantitatively characterize the wettability of each sample in different states, the relevant parameters of the four samples were inverted using the SA algorithm based on the dielectric dispersion model. The partial input and output parameters of the inversion were close to those ranges described in the above section. The radius of the hydrocarbon droplets r_0 was assumed to be 1 μm; its effect on X_w is minor.

Table 5 presents the parameter values obtained via inversion. The ion mobility of the electric double layer includes those of the Stern and diffuse layers. The ion mobilities of the two layers can differ by two orders of magnitude. Although the ion mobilities for samples A and B (or α and β) differed, the corresponding parameter values were close. No oil droplets were observed in samples ZY3-14B or ZY4-34β after cleaning and water saturation. Thus, the relevant parameters of the oil phase were not vital to the model. The grains, oil and water droplets were spherical; thus, the inverted depolarization factors were between 1/3 and 2/3. The inverse parameter values were substituted into the model to calculate

Table 4
Assumed and inverted values for comparison.

Parameter	Unit	Assumed value	Set range	Maximum	Minimum	Average (five times)
β_{ST}	m^2/sV	$5.2e^{-9}$	$0.1e^{-9}$–$10e^{-9}$	$6.2e^{-9}$	$1e^{-9}$	$5.6e^{-9}$
β_0	m^2/sV	$5.2e^{-8}$	$0.1e^{-8}$–$10e^{-8}$	$6.9e^{-8}$	$1.2e^{-8}$	$4.8e^{-8}$
α_{ST}	/	1.5	0.1–5	1.62	1.34	1.49
α_0	/	4	0.1–5	4	3.3	3.82
r	μm	90	1–100	99	80	89.9
$\varepsilon_{HC,C}$	/	1/3	0.3–0.7	0.44	0.31	0.36
N_f	/	1/3	0.3–0.7	0.40	0.33	0.34
N_g	/	1/3	0.3–0.7	0.41	0.33	0.35

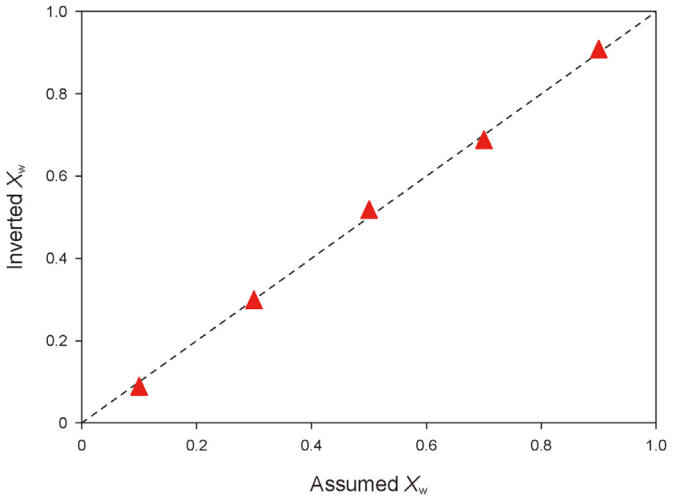

Fig. 8. Comparison of the assumed and inverted X_w values, which exhibits a good agreement.

permittivity curves for comparison with the measured values, as shown in Figs. 9 and 10. The error between the calculated and measured values was small, and the defined relative errors were all <10%, as shown in Table 5. In addition, the X_w range for each sample was narrow; thus, the uncertainty of X_w was small.

According to the inverted X_w values, sample ZY3-14A was oil-wet, and sample ZY3-14B after cleaning was water-wet. The X_w values of ZY4-34α and ZY4-34β were 0.39 and 0.41, respectively. The results indicate that cleaning changed the wettability to different degrees (Feng et al., 2017; Liang, 2019), which is consistent with the findings of the NMR T_2 spectra analysis.

For comparison, the relevant parameters of rock samples ZY2-16A and ZY5-3 were inverted, as shown in Table 5. Fig. 11 presents a comparison between the experimental and calculated values for samples ZY5-3 and ZY2-16A. The water saturation (S_w) of sample ZY5-3 after cleaning was 100%. The depolarization factor of the oil phase and other relevant parameters did not affect the rock's relative permittivity, and the X_w value was 0.99. The S_w of ZY2-16A was approximately 51%, and the X_w was 0.15. Therefore, the fractional wettability index X_w obtained from the inversion of the two rock samples was consistent with the wettability results based on the NMR T_2 spectra. In addition, the relative permittivity of the water-wet ZY5-3 sample decreased more rapidly than that of the oil-wet ZY2-16A sample, which is consistent with the analysis above.

Many studies suggest that the Archie's saturation index n value of oil wet rocks is higher than that of water wet rock's (Sweeney and Jennings, 1960; Anderson, 1986; Moss et al., 1999; Mao et al., 1997). Generally, the n value of hydrophilic rocks is around 2, while the n value of lipophilic rocks is mostly between 2.5 and 10, with an extensive range of variation. Mungan and Moore (1968) established a quantitative linear relationship between the n values and the wettability of rocks using two sets of samples, which indicate the n values are affected by wettability. However, for the low-permeability samples, the resistivity could not accurately quantitatively reflect the rock wettability because the n values in this type of samples are affected by pore structure and wettability (Feng et al., 2017; Han et al., 2022). Fig. 12 presents a crossplot of the n values versus the fractional wettability index X_w. Notably, n was obtained experimentally from the same batch of samples used by Zhao et al. (2023). As shown, n decreased as X_w (for the water-wet surface) increased, and the correlation between these two indices was strong. The sample ZY3-14B with $n = 2.45$ is determined to be water-wet, which is because the permeability is low. The aforementioned results indicate that the X_w derived from the dielectric dispersion model is suitable for characterizing rock wettability, that

Table 5
Inversed parameters of the samples (uncertainty of X_w is < 0.01).

Samples	β_{ST}, m^2/sV	β_0, m^2/sV	α_{ST}	α_{S0}	R, m	N_g	$N_{HC,C}$	N_f	X_w	Relative error ($r_0 = 1$ μm)
ZY3-14A	$1.1e^{-9}$	$6.2e^{-8}$	0.113	1.727	$1.9e^{-5}$	0.667	0.442	0.333	0.23	3%
ZY4-34α	$1e^{-10}$	$1.71e^{-8}$	0.739	1.917	$1.5e^{-5}$	0.667	0.660	0.333	0.39	8%
ZY3-14B	$9.1e^{-10}$	$8.9e^{-8}$	0.058	1.155	$2.0e^{-5}$	0.667	/	0.333	0.99	9%
ZY4-34β	$2.01e^{-10}$	$1.8e^{-8}$	0.662	1.138	$1.5e^{-5}$	0.61	/	0.362	0.41	6%
ZY2-16A	$5e^{-10}$	$2.2e^{-8}$	0.11	1.77	$9.0e^{-5}$	0.333	0.332	0.333	0.15	3%
ZY5-3	$2.1e^{-10}$	$5.2e^{-8}$	0.114	1.212	$2.98e^{-5}$	0.333	/	0.333	0.99	5%

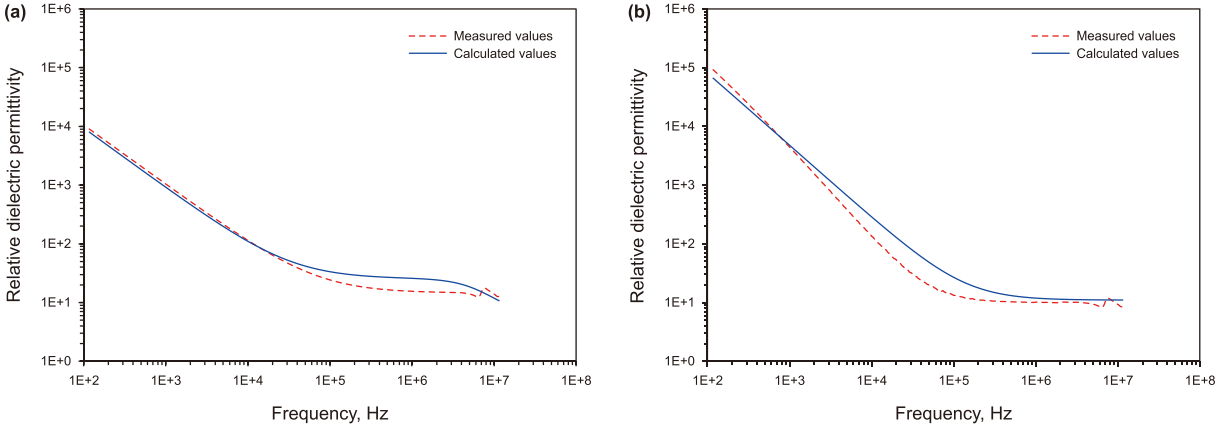

Fig. 9. Comparison between experimental (red dashed lines) and calculated (blue lines) values for samples ZY3-14A and ZY3-14B, which were non-cleaned and cleaned, respectively. The measured and calculated values agree well. **(a)** ZY3-14A. **(b)** ZY3-14B.

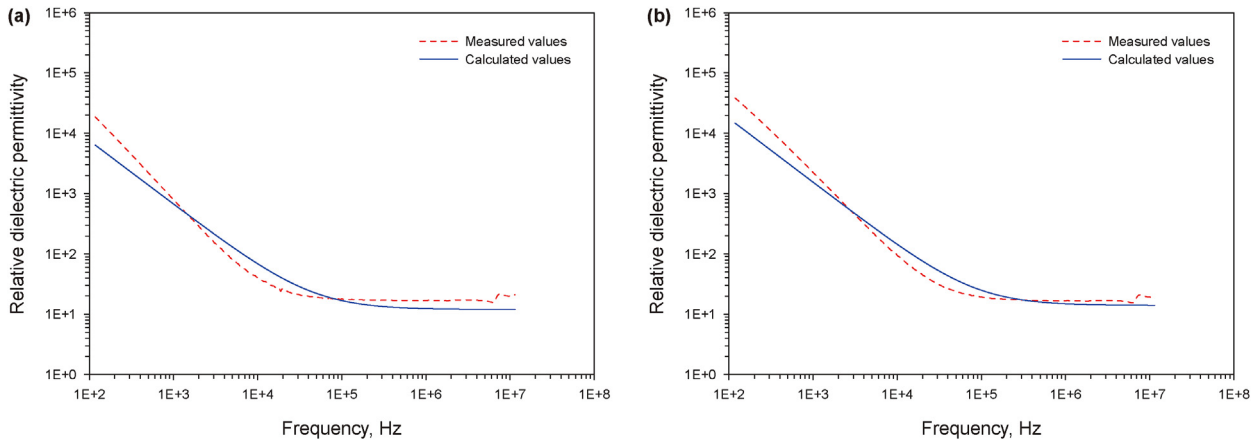

Fig. 10. Comparison between experimental (red dashed lines) and calculated (blue lines) values for samples ZY4-34α and ZY4-34β, which were non-cleaned and cleaned, respectively. The measured and calculated values agree well. **(a)** Sample ZY4-34α. **(b)** Sample ZY4-34β.

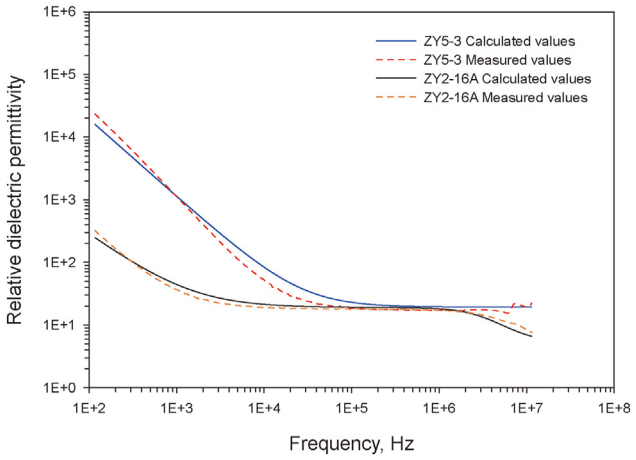

Fig. 11. Comparison between experimental and calculated values for samples ZY2-16A and ZY5-3, which were non-cleaned and cleaned, respectively. The measured and calculated values agree well.

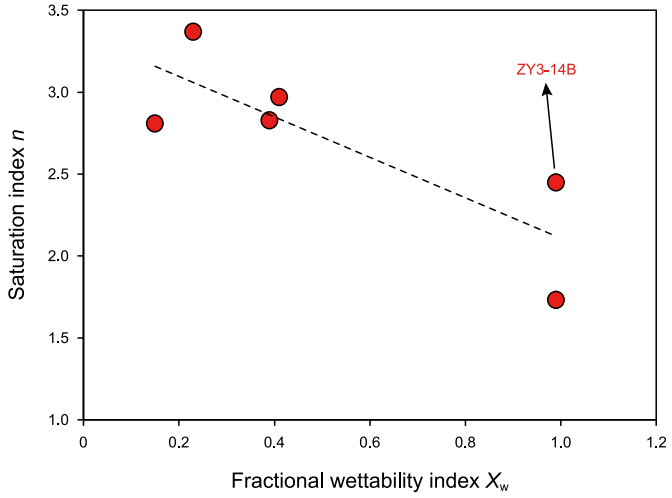

Fig. 12. Crossplot of the saturation index versus the fractional wettability index X_w. The n decreased as X_w (for the water-wet surface) increased, indicating a strong correlation between the two parameters.

the inversion results are effective.

5. Discussion

Three physical methods were used to characterize the rock wettability qualitatively and quantitatively: NMR spectroscopy, dielectric dispersion measurements, and resistivity measurements. NMR spectra measured both in the laboratory and in boreholes can be used to indicate wettability. Those measured in boreholes can be qualitatively indicative. Because the NMR T_2 spectra are affected by the pore structure and pore fluids, they should be measured in different states to obtain helpful information regarding wettability. Regarding the resistivity, the saturation index n-values are commonly used to indicate the wettability in conventional reservoir rocks. Except for sample ZY3-14B, the samples studied had medium-high porosity and permeability, and the saturation index is primarily affected by the wettability. The inverted X_w from low-frequency dielectric dispersion was consistent with the saturation index.

Although the rock wettabilities obtained from the three physical methods were strongly correlated, the dielectric model has too many uncertain parameters, and the imaginary parts of dielectric spectra were not considered in this study. It is imperative to improve or develop new models for characterizing the wettability of more complex rocks. Additionally, no traditional direct measurements were used to assess rock wettability in this study. In the future, the wettability should be measured using the traditional Amott index method, to evaluate further the effectiveness and reliability of the dielectric spectra for characterizing rock wettability.

6. Conclusions

A set of experimental schemes for obtaining rocks with different wettabilities was designed, and the dielectric and NMR T_2 spectra of lipophilic rocks were measured. Samples whose peak values of the T_2 spectra in the oil-displaced state were shifted left compared with those in the water-saturated state were characterized as oil-wet, whereas those whose peak values of the T_2 spectra in the oil-displaced state were shifted right or were not shifted compared with those in the water-saturated state were characterized as water-wet.

At frequencies below 10 kHz, the relative dielectric permittivities of rocks with different wettabilities differed significantly, and the permittivities of the water-wet samples exceeded those of the

oil-wet samples. The dielectric permittivities of the water-wet samples within the frequency range of 100 Hz–1 MHz declined more rapidly than those of the oil-wet samples.

According to the Garcia and Heidari dielectric dispersion model, X_w and other parameters were inverted using an SA method. The error between the modeling permittivities obtained using the inversion parameters and the experimental measurements was insignificant, indicating that the proposed method can be used to invert the dielectric dispersion data.

The X_w was consistent with the NMR T_2 spectra and Archie saturation index n, indicating that the dielectric dispersion can be used to characterize rock wettability accurately.

CRediT authorship contribution statement

Pei-Qiang Zhao: Writing – review & editing, Supervision, Methodology, Conceptualization. **Yu Chen:** Writing – original draft, Investigation. **Yu-Ting Hou:** Resources. **Xiu-Ling Chen:** Data curation. **Wei Duan:** Validation. **Shi-Zhen Ke:** Formal analysis.

Declaration of interest statement

The authors declare no conflict of interest.

Acknowledgments

This paper is supported by the Beijing Municipal Natural Science Foundation (1242025).

References

Al-Ofi, S., Sauerer, B., Dyshlyuk, E., Valori, A., Abdallah, W., 2017. Influence of rock wettability alteration on dielectric dispersion data. In: SPE Kingdom of Saudi Arabia Annual Technical Symposium and Exhibition. April 25, Dammam, Saudi Arabia. https://doi.org/10.2118/188028-ms.

Anderson, W.G., 1986. Wettability literature Survey-Part 3: the effects of wettability on the electrical properties of porous media. J. Petrol. Technol. 38 (12), 1371–1378. https://doi.org/10.2118/13934-PA.

Bona, N., Ortenzi, A., Capaccioli, S., 2002. Advances in understanding the relationship between rock wettability and high-frequency dielectric response. J. Petrol. Sci. Eng. 33 (1–3), 87–99. https://doi.org/10.1016/S0920-4105(01)00178-4.

Bona, N., Rossi, E., Capaccioli, S., 1999. Electrical measurements in the 100Hz-10GHz for efficient rock wettability evaluation. In: SPE International Symposium on Oilfield Chemistry. February 16, Houston, Texas, USA. https://doi.org/10.2118/50720-MS.

Bona, N., Rossi, E., Venturini, C., Capaccioli, S., 1998. Characterization of rock wettability though dielectric measurements. Rev. Inst. Fr. Petrol 53 (6), 771–783. https://doi.org/10.2516/ogst:1998068.

Börner, J.H., Herdegenb, V., Repkeb, J.U., Spitzer, K., 2015. The Spectral Complex Electrical Conductivity of the Three-phase System Sand/pore water/CO2 at Elevated Pressures and Temperatures. SEG Technical Program Expanded Abstracts, pp. 3129–3133. https://doi.org/10.1190/segam2015-5886074.1.

Butler, J.P., Reeds, J.A., Dawson, S.V., 1981. Estimating solutions of first kind integral equations with nonnegative constraints and optimal smoothing. SIAM J. Numer. Anal. 18 (3), 381–397. https://doi.org/10.1137/0718025.

Capaccioli, S., Lucchesi, M., Casalini, R., Rolla, P.A., Bona, N., 2000. Influence of the wettability on the electrical response of microporous systems. J. Phys. Appl. Phys. 33 (9), 1036–1047. https://doi.org/10.1088/0022-3727/33/9/302.

Chen, X., Yu, P., Zhang, L.L., Li, Y., Wang, J.L., 2011. Adaptive regularized synchronous joint inversion of MT and seismic data. Chin. J. Geophys. 54 (10), 2673–2681. https://doi.org/10.3969/j.issn.0001-5733.2011.10.024 (in Chinese).

Feng, C., Mao, Z.Q., Yin, W., Shi, Y.J., Zhang, B., Wang, X.H., li, G.R., 2017. Study on resistivity experiments and conductive mechanism in low-permeability reservoirs with complex wettability. Chin. J. Geophys. 60 (3), 1211–1220. https://doi.org/10.6037/cjg20170331 (in Chinese).

Feng, S., Sen, P.N., 1985. Geometrical model of conductive and dielectric properties of partially saturated rocks. J. Appl. Phys. 58 (8), 3236–3243. https://doi.org/10.1063/1.335804.

Garcia, A.P., Heidari, Z., Torres-Verdin, C., 2019. Multi-frequency interpretation of electric resistivity and dielectric permittivity measurements for simultaneous assessment of porosity, water saturation, and wettability. In: SPWLA 60th Annual Logging Symposium. June 15. The Woodlands, Texas, USA. https://doi.org/10.30632/T60ALS-2019_III.

Garcia, A.P., Heidari, Z., 2018. Integrated characterization of multi-frequency dielectric dispersion measurements in mixed-wet rocks. In: SPWLA 59th Annual Logging Symposium. June 02, London, UK.

Gkortsas, V.M., Venkataramanan, L., Ramakrishnan, T.S., Freed, D., 2015. Indication of wettability from dielectric measurements on partially saturated rocks using effective medium models. Geophysics 80 (5), E257–E265. https://doi.org/10.1190/GEO2015-0028.1.

Han, Y.J., Zhou, C., Li, C.L., Yu, J., Xu, H.J., 2022. Conductive response law of oil wet and water-wet sandstone in Ordos Basin under the influence of oil viscosity. Acta Pet. Sin. 43 (6), 829–839. https://doi.org/10.7623/syxb202206007 (in Chinese).

Hu, Q.H., Liu, H.M., Li, M.W., Li, Z., Yang, R., Zhang, Y.X., Sun, M.D., 2018. Wettability, pore connectivity and fluid-tracer migration in shale oil reservoirs of Paleogene Shahejie Formation in dongying sag of Bohai Bay Basin, east China. Acta Petrolei Sinaca 39 (3), 278–289. https://doi.org/10.7623/syxb201803003 (in Chinese).

Jia, H., Zhang, R., Luo, X.B., Zhou, Z.L., Yang, L., 2024. Nuclear magnetic resonance experiment on the time-varying law of oil viscosity and wettability in high multiple waterflooding sandstone core. Petrol. Explor. Dev. 51 (2), 348–355. https://doi.org/10.11698/PED.20230069.

Jiang, X.D., Wang, W.R., 2024. The probabilistic determination of lunar subsurface fault structure across the mare Crisium by very fast simulated annealing (VFSA) approach. Geosci. Rem. Sens. Lett. IEEE 21, 1–5. https://doi.org/10.1109/LGRS.2024.3454385.

Jin, Y.T., Misra, S., Homan, D., 2020b. Estimation of in-situ wettability using multi-frequency electromagnetic measurements. In: Unconventional Resources Technology Conference. July 20. Virtual. https://doi.org/10.15530/urtec-2020-2928.

Jin, Y.T., Misra, S., Homan, D., Rasmus, J., 2020a. Effects of wettability of conductive particles on the multifrequency conductivity and permittivity of fluid-filled porous material. Fuel 268, 117411. https://doi.org/10.1016/j.fuel.2020.117411.

Knight, R.J., Abad, A., 1995. Rock/water interaction in dielectric properties: experiments with hydrophobic sandstones. Geophysics 60 (2), 431–436. https://doi.org/10.1190/1.1443780.

Kuang, L.C., Wang, Z.L., Feng, C., Zhao, P.Q., Mao, R., Yu, J., 2020. Predicting oil saturation of shale-oil reservoirs using nuclear magnetic resonance logs. Interpretation 8 (3), SL35–SL43. https://doi.org/10.1190/int-2019-0150.1.

Li, J.J., Ke, S.Z., Yin, C.F., Zheng, M.K., 2019. A laboratory study of complex resistivity spectra for predictions of reservoir properties in clear sands and shaly sands. J. Petrol. Sci. Eng. 177, 983–994. https://doi.org/10.1016/j.petrol.2019.01.061.

Liang, C., 2019. Study on Magnetic Resonance Relaxation Characterizing Rock Wettability. Doctor Dissertation, China University of Petroleum (Beijing). https://doi.org/10.27643/d.cnki.gsybu.2019.000150

Liang, C., Jia, Z.J., Xiao, L.Z., 2023a. Review on nuclear magnetic resonance characterization for rock wettability. Prog. Geophys. 38 (4), 1610–1624. https://doi.org/10.6038/pg2023GGO485 (in Chinese).

Liang, C., Xiao, L.Z., Jia, Z.J., G, L., Luo, S.H., Wang, Z.Y., 2023b. Mixed wettability modeling and nuclear magnetic resonance characterization in tight sandstone. Energy&Fuels 37 (3), 1962–1974. https://doi.org/10.1021/acs.energyfuels.2c03720.

Looyestijn, W., Hofman, J., 2005. Wettability index determination by nuclear magnetic resonance. In: SPE Middle East Oil and Gas Show and Conference. https://doi.org/10.2118/93624-PA.

Looyestijn, W.J., Hofman, J., 2008. Wettability index determination from NMR logs. Petrophysics 49, 130–145. https://doi.org/10.2118/93624-MS.

Mao, Z.Q., Zhang, C.G., Lin, C.Z., 1997. The effect of wettability of reservoir on the log-derived water saturation. Well Logging Technol. 21 (1), 50–55. https://doi.org/10.16489/j.issn.1004-1338.1997.01.008 (in Chinese).

Metropolis, N., Rosenbluth, A.W., Rosenbluth, M.N., Teller, A.H., Teller, E., 1953. Equation of state calculations by fast computing machines. J. Chem. Phys. 21 (6), 1087–1092. https://doi.org/10.1063/1.1699114.

Moss, A.K., Jing, X.D., Archer, J.S., 1999. Laboratory investigation of wettability and hysteresis effects on resistivity index and capillary pressure characteristics. J. Petrol. Sci. Eng. 24 (2–4), 231–242. https://doi.org/10.1016/S0920-4105(99)00045-5.

Mungan, N., Moore, E.J., 1968. Certain wettability effects on electrical resistivity in porous media. J. Can. Petrol. Technol. 7, 20–25. https://doi.org/10.2118/68-01-04.

Netto, A., Dunbar, J., 2019. 3-D constrained inversion of gravimetric data to map the tectonic terranes of southeastern Laurentia using simulated annealing. Earth Planet Sci. Lett. 513, 12–19. https://doi.org/10.1016/j.epsl.2019.02.018.

Newgord, C., Garcia, A.P., Heidari, Z., 2019. A new method to quantify wettability from resistivity measurements: workflow development and experimental core-scale verification. In: SPE Europec Featured at 81st EAGE Conference and Exhibition. June 03, London, England, UK. https://doi.org/10.2118/195565-MS.

Newgord, C., Garcia, A.P., Rostami, A., Heidari, Z., 2018. Improved interpretation of electrical resistivity measurements in mixed-wet rocks: an experimental core-scale application and model verification. Petrophysics 59, 703–718. https://doi.org/10.30632/PJV59N5-2018a9.

Nguyen, B.L., Bruining, J., Slob, E.C., 1999. Effects of wettability on dielectric properties of porous media. SPE Annual Technical Conference and Exhibition. In: SPE Annual Technical Conference and Exhibition. October 03, Houston, Texas, USA. https://doi.org/10.2118/56507-MS.

Niu, Q.F., Revil, A., 2016. Connecting complex conductivity spectra to mercury porosimetry of sedimentary rocksInduced polarization and pore sizes. Geophysics 81 (1), E17–E32. https://doi.org/10.1190/geo2015-0072.1.

Niu, Q.F., Zhang, C., Prasad, M., 2020. A framework for pore-scale simulation of effective electrical conductivity and permittivity of porous media in the

frequency range from 1 mHz to 1 GHz. Journal of Geophysical Research: Solid Earth 125, e2020JB020515. https://doi.org/10.1029/2020JB020515.
Prasad, S.N., 1999. An inversion of geomagnetic deep sounding data using simulated annealing. Phys. Earth Planet. Inter. 110, 129–135. https://doi.org/10.1016/s0031-9201(98)00155-1.
Revil, A., Leroy, P., 2004. Constitutive equations for ionic transport in porous shales. J. Geophys. Res. Solid Earth 109, B03208. https://doi.org/10.1029/2003JB002755.
Seleznev, N.V., Habashy, T.M., 2016. Determining formation wettability from dielectric measurements. U.S. Patent 9 (291), 050. 2016-3-22.
Stogryn, A., 1971. Equations for calculating the dielectric constant of saline water (Correspondence). IEEE Trans. Microw. Theor. Tech. 19 (8), 733–736. https://doi.org/10.1109/TMTT.1971.1127617.
Sweeney, S.A., Jennings, H.Y., 1960. Effect of wettability on the electrical resistivity of carbonate rock from a petroleum reservoir. J. Phys. Chem. 64 (5), 551–553. https://doi.org/10.1021/j100834a009.
Tong, Z.M., 2016. Analysis of Jurassic Residual Oil Reservoir Genesis and Log Characteristics in Ordos Basin. Master Dissertation. China University of Petroleum (Beijing) (in Chinese).
Toumelin, E., Torres-Verdin, C., Bona, N., 2005. Improving the petrophysical assessment of rock-fluid systems with wide-band electromagnetic measurements. In: SPE Annual Technical Conference and Exhibition. October 09, Dallas, Texas. https://doi.org/10.2118/96258-MS.
Wang, Y.L., 2022. Identification and Evaluation Method of Jurassic Complex Oil Layers and Water Layers in Western Margin of Ordos Basin. Master Dissertation. China University of Petroleum (Beijing). https://doi.org/10.27643/d.cnki.gsybu.2022.000707 (in Chinese).
Wei, R., Xu, W., Li, H., Yan, Z.H., Zheng, Y.P., Ke, S.Z., Zhao, P.Q., 2024. Evaluation method of tight sandstone reservoir saturation based on frequency domain electrical dispersion measurement data. Geoenergy Science and Engineering 241, 212977. https://doi.org/10.1016/j.geoen.2024.212977.
Xu, Z.Y., Liao, X., Liu, L.H., Fu, N.Y., Fu, Z.H., 2023. Research on small-loop transient electromagnetic method forward and nonlinear optimization inversion method. IEEE Trans. Geosci. Rem. Sens. 61, 1–13. https://doi.org/10.1109/tgrs.2023.3237842.
Zhao, P.Q., Zeng, L.B., Hou, Y.T., Hu, C., Wang, Y.L., He, W., Mao, Z.Q., 2023. Experimental measurements and response analysis of resistivity of reservoirs with complex wettability: a case study of Yan'an Formation, Ordos Basin, China. Geophysics 88 (5), B195–B206. https://doi.org/10.1190/geo2022-0456.1.
Zhou, H.Y., Mo, X.W., Wang, L.L., Xu, B.Y., 2021. The research of the slowness extraction method of component waves in array acoustic logging data based on simulated annealing algorithm. Geophys. Geochem. Explor. 45 (2), 466–472. https://doi.org/10.11720/wtyht.2021.2472 (in Chinese).